Analysis of Receptor Clustering on Cell Surfaces by Imaging Fluorescent Particles

Ian E. G. Morrison,* Catherine M. Anderson,* George N. Georgiou,* Gregory V. W. Stevenson,‡ and Richard J. Cherry*

*Department of Chemistry and Biological Chemistry, University of Essex, Wivenhoe Park, Colchester CO4 3SQ, and ‡Rhone Poulenc Rorer, Rainham Road South, Dagenham, Essex RM10 7XS, United Kingdom

ABSTRACT Fluorescently labeled low density lipoproteins (LDL) and influenza virus particles were bound to the surface of human fibroblasts and imaged with a cooled slow-scan CCD camera attached to a fluorescence microscope. Particles were also imaged after attachment to polylysine-coated microscope slides. The digital images were analyzed by fitting data points in the region of fluorescent spots by a two-dimensional Gaussian function, thus obtaining a measure of spot intensity with correction for local background. The intensity distributions for particles bound to polylysine slides were mainly accounted for by particle size distributions as determined by electron microscopy. In the case of LDL, the intensity distributions for particles bound to fibroblasts were considerably broadened, indicative of clustering. The on-cell intensity distributions were deconvolved into 1-particle, 2-particle, 3-particle, etc. components using the data obtained with LDL bound to polylysine-coated slides as an empirical measure of the single particle intensity distribution. This procedure yielded a reasonably accurate measure of the proportion of single particles, but large errors were encountered in the proportions of larger cluster sizes. The possibility of studying the dynamics of clustering was investigated by binding LDL to cells at 4°C and observing changes in the intensity distribution with time after warming to 20°C.

INTRODUCTION

Integral membrane proteins are able to diffuse to a greater or lesser extent within the plane of the membrane and, hence, have the potential to vary their state of aggregation. Microaggregation of receptors in response to, for example, hormones, growth factors, or antibodies provides an important method of transmembrane signaling (Bormann and Engelman, 1992; Metzger, 1992). In addition, entrapment and clustering of receptors in coated pits is the initial step in the internalization of a wide variety of ligands by receptor-mediated endocytosis (Goldstein et al., 1979).

Although fluorescence microscopy is a powerful technique for studying the behavior of receptors on the surfaces of living cells, it lacks the spatial resolution to determine the size of receptor clusters. A method of overcoming this limitation was introduced by Gross and Webb (1986) and is based on an imaging system of sufficient sensitivity to detect individual ligands. This is feasible for ligands such as LDL of sufficient size to incorporate a few tens of fluorescent molecules. LDL particles have a diameter of 20–25 nm and consist of a core of cholesterol esters bound by a monolayer containing phospholipids, free cholesterol, and a single protein apoprotein B-100 (Hillyard et al., 1955; Kane, 1983). Barak and Webb (1981) first showed that LDL readily incorporates the fluorescent lipid analog dil (1,1-dioctadecyl-3,3,3′,3′-tetramethylindocarbocyanine) and that individual LDL particles labeled with about 40 probes can be visualized in the fluorescence microscope using an image-intensified video camera.

To investigate receptor clustering, Gross and Webb (1986) analyzed the fluorescence intensity distribution of dil-labeled LDL bound to fibroblasts. They observed a series of equally spaced peaks in the distribution, which they assigned to clusters of 1, 2, 3, etc. LDL particles; the widths of the peaks were assumed to be controlled by a Poissonian variation in the number of probes/particle. The data were thus interpreted to provide a quantitation of the distribution of LDL particles (and hence their receptors) between different sized clusters.

Clearly, this technique is potentially of great value for studying receptor microaggregation on the surfaces of living cells. Here we further investigate the approach by employing a cooled slow-scan charge-coupled device (CCD) camera for the imaging system and developing an improved method of quantitating the intensities of individual fluorescent spots. The CCD detector provides high sensitivity, wide dynamic range, and lack of geometric distortion (Hiraoka et al., 1987). In addition to a static analysis of cluster size distribution, we have also investigated the possibility of observing time-dependent clustering with this imaging system.

We have studied LDL labeled with two different fluorescent probes and also influenza virus. These virus particles are larger than LDL (~100 nm in diameter) and are enveloped by a lipid bilayer that also readily incorporates lipophilic probes such as octadecyl-rhodamine (R_{18}) (Hoekstra et al., 1984). A preliminary account of part of the present studies with LDL was previously reported (Anderson et al., 1989).

Received for publication 11 February 1994 and in final form 13 June 1994.

Address reprint requests to Richard J. Cherry, Department of Chemistry and Biological Chemistry, University of Essex, Wivenhoe Park, Colchester CO4 3SQ United Kingdom. Tel.: 011-44-206-872244; Fax: 011-44-206-873598; E-mail: cherr@essex.ac.uk.

0006-3495/94/09/1280/11 $2.00

MATERIALS AND METHODS

Cells

Human dermal fibroblasts (D532 and JD) were obtained from Flow Laboratories (Rickmansworth, UK). The cells were grown in Dulbecco's Modified Eagle's Medium (DMEM) containing 10% fetal calf serum and supplemented with penicillin G (100 units/ml), streptomycin sulphate (100 μg/ml) and L-glutamine (2 mM). Cells were grown at 37°C in 7% CO_2. For imaging experiments, trypsinised cells were seeded onto 8 well Lab-Tek slides (Gibco, Paisley, UK) and cultured for a further 96 h. For LDL experiments, LDL receptors were up-regulated by incubating cells in lipoprotein-deficient growth medium during the last 48–72 h, essentially as described by Brown et al. (1974).

LDL and influenza virus

LDL was prepared from freshly drawn human blood by sequential flotation ultracentrifugation (Hatch and Lees, 1968). The purity of the preparation was confirmed by agarose gel electrophoresis. Samples were stored in 150 mM NaCl, 10 mM Tris, 1 mM EDTA, pH 7.4 before use. Influenza virus, strain X47, grown in embryonated chicken eggs was generously provided by Professor C. Pasternak (St. Georges Hospital Medical School).

Labeling with fluorescent probes

LDL was labeled with either DiI or R_{18} from Molecular Probes, Inc. (Eugene, OR). The probe was solubilized in dimethyl sulphoxide (1.7 mM), and 120 μl of the solution was incubated with 1.21 mg of LDL in approximately 400 μl for 1 h at 37°C under nitrogen. Labeled LDL was separated from free probe on a Pharmacia PD10 column eluted with 150 mM NaCl, 10 mM Tris, 1 mM EDTA, pH 7.4, and stored at 4°C. Protein was determined by the method of Markwell et al. (1978) and probe concentration by absorbance measurement assuming extinction coefficients of 117,000 cm^{-1} M^{-1} for DiI and 93,000 cm^{-1} M^{-1} for R_{18} (Haugland, 1989). The average number of probes per LDL particle was calculated assuming that protein constitutes 25% by weight of LDL and the average molecular mass of the particles is 2.75×10^6 Daltons (Goldstein and Brown, 1977). Labeling ratios were typically found to be 30–50 probes/LDL particle.

Influenza virus was labeled with R_{18} essentially as described by Hoekstra et al. (1984). Protein concentration was determined according to Lowry et al. (1951) and probe concentration by optical absorbance. The average number of probes per virus particle was calculated using a conversion factor of 1.75×10^{12} virus particles per mg of protein. The labeling conditions were adjusted to give final labeling ratios in the range 100–1000 probes per virus particle.

Electron microscopy

LDL or influenza virus was dialysed overnight at 4°C against 2.6 mM ammonium carbonate and 0.125 M ammonium acetate, pH 7.4. After dialysis, the sample was filtered through a 200 nm pore filter and diluted to approximately 0.2 mg protein/ml. A drop of the sample was applied to a 400 mesh formvar carbon-coated copper grid and allowed to settle for approximately 30 s. The sample was blotted, 1% phosphotungstic acid, pH 7.4 applied for a few s, and then blotted again. The grid was allowed to dry and then viewed using a Jeol 200cx transmission electron microscope at an accelerating voltage of 200 kV.

Fluorescence microscopy

D532 cells on Lab-Tek slides were labeled with fluorescent LDL at 4°C using a procedure modified from that described by Barak and Webb (1981). Chilled cells were washed 3 times in phosphate-buffered saline (PBS) and then once in DMEM supplemented with 10 mM HEPES and 2 mM Ca^{2+} at pH 7.4 (buffer A). Labeled LDL was diluted to 50 μg/0.45 ml in buffer A. Cells were incubated at 4°C with labeled LDL at this concentration for either 2 h for experiments with fixed cells or 10–30 min for experiments with live cells. They were then washed 3 times in PBS supplemented with 2 mM Ca^{2+} and incubated for 10 min in PBS supplemented with 2 mM Ca^{2+}, 2 mg/ml BSA and 10 mM Tris at pH 7.4 For experiments with live cells, the cells were washed once more in buffer A, and the slides were transferred to the microscope stage maintained at 4°C. Otherwise, cells were fixed in 3% formaldehyde for 10 min at 4°C and 15 min at room temperature and washed once in PBS before microscopy. Nonspecific binding was checked by incubating cells with labeled LDL in the presence of a 10-fold excess of unlabeled LDL. Similar procedures were used with influenza virus except that the incubation and washing buffers consisted of 137 mM NaCl, 2.7 mM KCl, and 10 mM phosphate buffer pH 7.4 and the incubation time was 5 min.

Polylysine-coated slides were prepared by cleaning glass microscope slides with concentrated nitric acid, rinsing with distilled water, and incubating for 5 min in 0.01% poly-L-lysine solution at room temperature. After incubation, slides were drained and dried in an oven. A drop of a suspension of labeled LDL (250 ng protein/ml) in 50 mM sodium barbitone, 1 mM EDTA pH 8.6 or of influenza virus in PBS was allowed to settle on the slide for 5 min. After rinsing with distilled water, the coverslip was mounted using a silicone grease ring and distilled water.

Temperature control of the slides during microscopy was by dual thermocirculators pumping water through a slideholder fitted with a thermocouple, placed under a plastic hood on the microscope stage. A suitable fibroblast was selected while the slide was maintained at 4°C, and the water flow was then switched to the second thermocirculator, set to 20°C, if ambient conditions were required. The change in temperature was completed in less than 2 min.

Fluorescence digital imaging microscopy was performed using a Nikon Diaphot inverted fluorescence microscope. The objective was a 40x phase contrast lens with numerical aperture 0.55; this provides lower resolution than a higher magnification objective, but the depth response of 1.5 μm ensures that surface irregularities stay in focus. Illumination was by a 50 W mercury lamp, and wavelengths were selected using Omega Optical Inc. filters and dichroic mirrors. For dil observations, 525 and 575 nm filters were placed in the excitation and emission beams, respectively, and the dichroic mirror cutoff was 545 nm. For R_{18} observations, the filters were 540 and 590 nm, and the dichroic mirror cutoff was 580 nm.

The CCD camera (Wright Instruments, Enfield, UK) was attached to the video port of the microscope, and the image was focused with a Hanimex f2.8 wide angle lens on to the EEV P8603 detector (576 × 384 pixels). This device has a maximum quantum efficiency of around 35% and a mean readout noise equivalent to 7 electrons/pixel. Image acquisition, storage, and display were performed using the Wright Instruments AT1 image control software, running on an IBM-AT compatible computer equipped with Wright Instruments image store and display cards. Images were typically recorded every 3 to 6 min with an exposure time up to 10 s.

Spot position and intensity determination

Individual LDL or virus particles and small clusters thereof have dimensions less than the resolution of an optical microscope. The intensity distribution in the diffraction-limited images of these particles is a Bessel function (see Inoue (1989) for a discussion of imaging small particles). To simplify the image analysis, we have approximated the distribution by a Gaussian function; the shapes of the two functions are very similar in the central peak. Least-squares fitting of the area around each spot with a two-dimensional Gaussian function (Fig. 1) allows the accurate assessment of peak height Z_s above local background Z_o, for a spot with position coordinates (X_s, Y_s) and width W_s, i.e.,

$$f(x, y) = Z_o + Z_s \exp\{-[(x - X_s)^2 + (y - Y_s)^2]/W_s^2\}. \quad (1)$$

The data values are the pixel contents from a square box drawn around the estimated peak center, the box size being chosen to give the best compromise between speed (small box, background poorly defined) and accuracy (large box, background may become nonuniform).

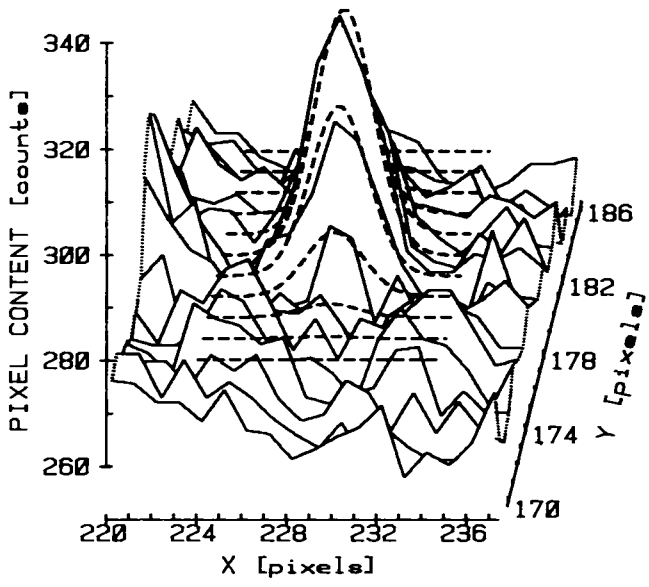

FIGURE 1 Three-dimensional representation of an 18-pixel square of data from a CCD camera image of fluorescently labeled LDL bound to a fibroblast. The solid lines link pixels in the X-direction; this area shows nonuniform background (sloping down left-to-right and front-to-back) and effects from a nearby fluorescent particle on the left. The central peak can be quantitated by least-squares fitting a two-dimensional Gaussian (– – –) to a 11x11 pixel area around the spot; scale 205 nm/pixel.

Spot positions were estimated by a simple image analysis algorithm to identify peaks having approximately the diffraction limited width. Fitting closely spaced spots was done in two ways:

(i) If another spot lies just outside the optimal box, then a circle was taken around this spot with radius equal to half the inter-spot distance. Pixels inside both the circle and the optimal box were ignored.
(ii) When another spot falls within the optimal box, the box size was increased to include both spots, which were fitted simultaneously with a combined function having independent heights and widths. Up to nine spots in a close group could be fitted in this way with separations down to ~2 pixel or about 400 nm at the magnification used.

Artefact rejection procedures

Artefacts in the fluorescence image can be caused by scattering of the excitation light at abrupt changes of optical density—e.g., dust particles, bubbles, etc.—and by electronic noise. Complete rejection of artefacts is obviously not possible, but three methods are used to try to isolate these interferences: selection by (a) spot width (b) width standard deviation (c)goodness-of-fit, or chi-squared.

The two-dimensional Gaussian fit provides values for the adjustable parameters, SEs for these, and the goodness-of-fit for each spot. When a frequency distribution is constructed for the spot widths, using data from a polylysine-coated slide where artefacts should be minimized, then an approximately normal distribution is seen (Fig. 2 *A*) and analyzed to obtain the mean μ_w and SD σ_w. Spots having widths outside the range $\mu_w \pm 2\sigma_w$ are rejected; the smaller values are from, e.g., cosmic rays, the larger from scattering artefacts. The $1/e$ half-width is 432 ± 80 nm, about 40% higher than the theoretical minimum for the optical system employed.

Histograms of spot width error and chi-squared are long-tailed (Fig. 2, *B* and *C*); the distribution of values beyond the most frequent can be analyzed to obtain a high-end cutoff point in a similar way to the width discrimination. Spots having large width errors are often "close doubles," and could be fitted as such, but it was deemed safer to omit them altogether. The test using goodness-of-fit values detects relatively few artefacts.

Intensity distribution analysis

A histogram with k data bins, typically 50–100, was created from the integrated fluorescence signal values $F_s = \pi W_s^2 Z_s$ of spots that satisfy the above criteria; this histogram distribution H_j was fitted by least squares to one of a variety of functions:

- normal distribution $H_j = N \exp\{-\frac{1}{2}[(F_j - F_{max})/w]^2\}$ (2)
- log normal distribution $H_j = N \exp\{-[\log(F_j - F_{max})/w]^2\}$ (3)
- radial distribution $H_j = N^* 2F_j/\sqrt{F_{max}} \exp\{-[F_j/F_{max}]^2\}$. (4)

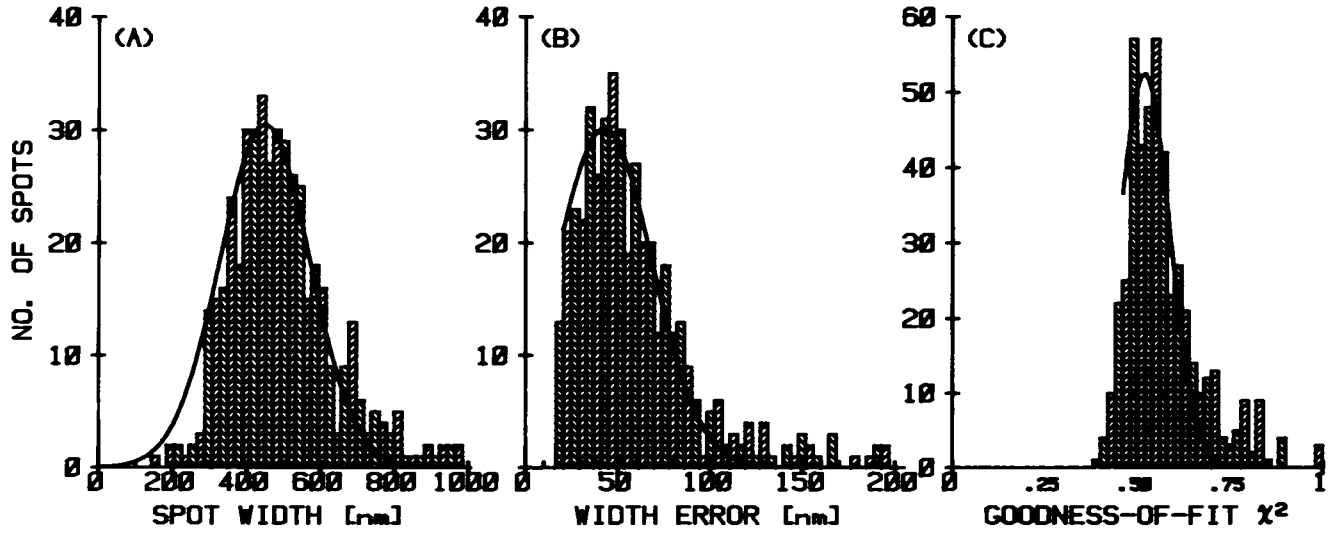

FIGURE 2 Distribution of parameters obtained by least-square fitting of spots in a fluorescence image of R_{18}-LDL particles dispersed on a polylysine-coated slide. (*A*) Spot widths; best-fit normal distribution (——) gives most probable $\mu_w = 2.1$ with SE $\sigma_w = 0.4$ pixels. (*B*) Spot width SDs; the single-sided normal distribution has $\mu_e = 0.12$ with SE $\sigma_e = 0.18$ pixels. (*C*) Goodness-of-fit χ^2; the single-sided normal distribution has most probable $\mu_\chi = 0.52$ with SE $\sigma_\chi = 0.14$.

Here N is the number of spots, divided by the normalizing factor required to have the integral of the function equal to N. In all cases, 2-particle cluster, 3-particle cluster, etc. distributions can be calculated by convolving the 1-particle distribution with itself to obtain the 2-particle distribution, the 2-particle with the 1-particle distribution to obtain the 3-particle distribution, and so on. Thus, for the normal distribution of 2-particle clusters

$$G_{2,j} = \sum_{i=1,j} \exp\{-\tfrac{1}{2}[(F_i - F_{max})/w]^2\} \exp\{-\tfrac{1}{2}[(F_{j-i} - F_{max})/w]^2\}. \quad (5)$$

Data can be tested against sums of these convolutions, variable parameters being the position of the 1-particle intensity maximum F_{max}, its width w and the total number of spots under each cluster size distribution.

Weighting of the data values in these fits is critical. Poisson-type weighting, assigning $\sqrt{H_j}$ as the weight for H_j but using weight 1 for zero values, gives visually inadequate fits. Unit weighting of all data values gave very similar fit parameters to a robust weighting scheme (Mosteller and Tukey, 1977), which zero-weights outlier values and, hence, gives smaller SEs for the variable parameters. The unit weighting scheme was preferred to avoid biasing the results by this outlier removal.

Time-dependent distributions: global analysis

Photobleaching of the fluorophores during successive camera exposures and any slight variations between imaging conditions combine to change the value of the intensity distribution maximum. To compensate for this, an intensity adjustment factor f_m was calculated for each image m by first identifying spots on the cell that are isolated and, thus, can be tracked through the images with confidence. The intensity ratios $Z_{n,m}/Z_{n,1}$ were then averaged for these spots (with outlier removal) to give the factor f_m.

The intensity histograms from all the images of the sequence were then fitted simultaneously by a sum of g log-normal convolutions as

$$H_{j,m} = N_{1,m}\exp\{-[\log(F_{j,m} - f_m F_{max})/w]^2\} + \sum_{i=2,g} N_{i,m} G_{i,j} \quad (6)$$

by global analysis (Knutson et al., 1983). In this method, F_{max} and w were global parameters applying to all m histograms, the number of spots in the ith cluster of the mth image ($N_{i,m}$) were individual, and f_m was the fixed experimentally determined value. The fitted values of N were converted into single-particle fractions $N_{1,m}/\Sigma N_{i,m}$ and plotted as a function of time.

RESULTS AND ANALYSIS

Particles bound to polylysine-coated slides

The fluorescence intensity distribution of populations of LDL and influenza virus particles was determined after binding them to polylysine-coated microscope slides. Fig. 3 shows data for LDL labeled with two different fluorescent probes and for virus with two different probe labeling ratios. In the case of virus, a fivefold increase in probe concentration results in only about a twofold increase in peak fluorescence intensity, which is indicative of self-quenching. Fig. 3 also shows the theoretical Poisson distributions of the number of

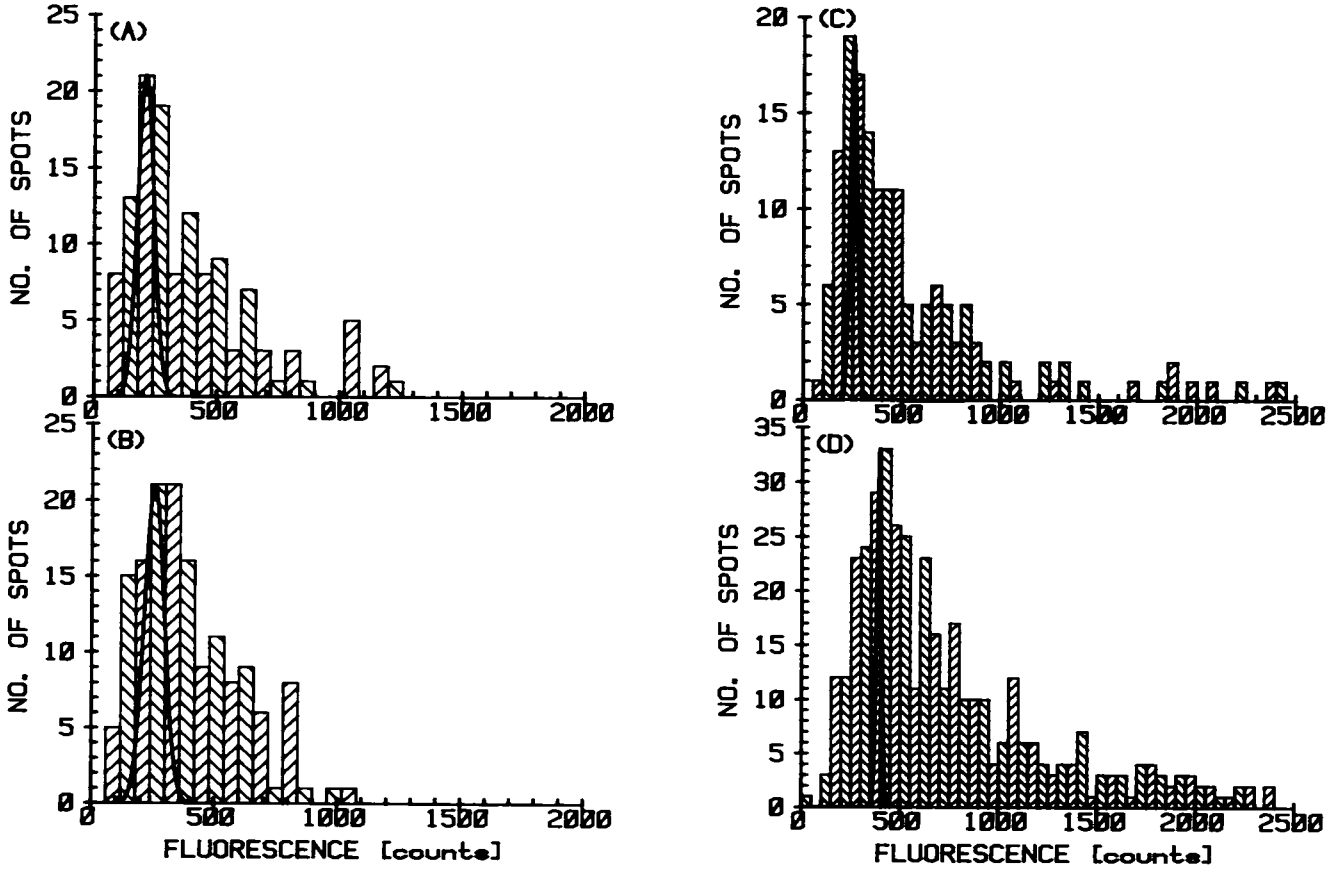

FIGURE 3 Distributions of fluorescence intensity for labeled particles on polylysine-coated slides. The CCD images were analyzed as described in the text, and the total intensity under the 2D-Gaussian profile was calculated from the fitted parameters (for each spot that satisfied the three conditions illustrated in Fig. 2). The solid lines represent Poisson profiles calculated from the known mean number of fluorophores/particle (with no allowance for self-quenching), centered on the most probable value in the intensity distribution. (*A*) LDL labeled with ~40 fluorophores/particle of diI. (*B*) LDL with ~40 R_{18}. (*C*) Virus with ~200 R_{18}. (*D*) Virus with ~1000 R_{18}.

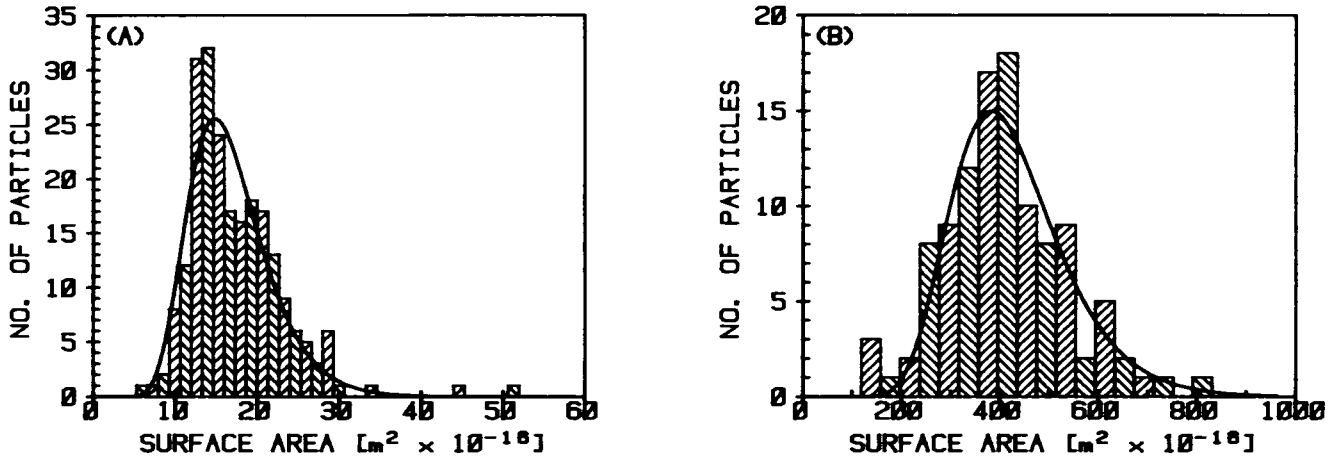

FIGURE 4 Distributions of particle surface areas of (*A*) LDL and (*B*) virus. Areas were calculated as $4\pi r^2$ from the particle mean radius r, measured in electron micrographs. The solid lines are best-fit log-normal distributions (the double-peaked distribution of LDL particles is not reproducible).

probes per particle in each case. Clearly, the measured fluorescence intensity distributions are much broader than the Poisson distributions.

Electron microscopy

The appearance of LDL and influenza virus particles in electron micrographs of negatively stained specimens was essentially the same as in published micrographs (Forte et al., 1968; Webster et al., 1992). Particle diameters were measured for labeled LDL and virus from which surface areas were calculated and binned into the histograms shown in Fig. 4. The diameter histograms did not approximate to a normal distribution and appeared to be long tailed; thus, the surface area distributions cannot be associated with a theoretical curve and so were fitted by a log-normal distribution, which gives a reasonable fit and is useful for comparison with the fluorescence intensity data. To further the comparison, the fluorescence intensity distributions in Fig. 3 were also fitted by a log-normal distribution (Eq. 3). Again, this has no theoretical foundation, but the distribution is long-tailed, whereas the radial distribution (Eq. 4) has no independent width parameter and so is less flexible. After normalization to the same peak value, these distributions are superimposed in Fig. 5.

Particles bound to fibroblasts

Fluorescence intensity distributions were determined for LDL or influenza virus bound to the surface of dermal fibroblasts. The results are shown in Fig. 6. Initially, data were obtained with fixed cells, but subsequently we preferred to work with unfixed cells at 4°C. Although very slow lateral diffusion persists at 4°C (Anderson et al., 1992), the time

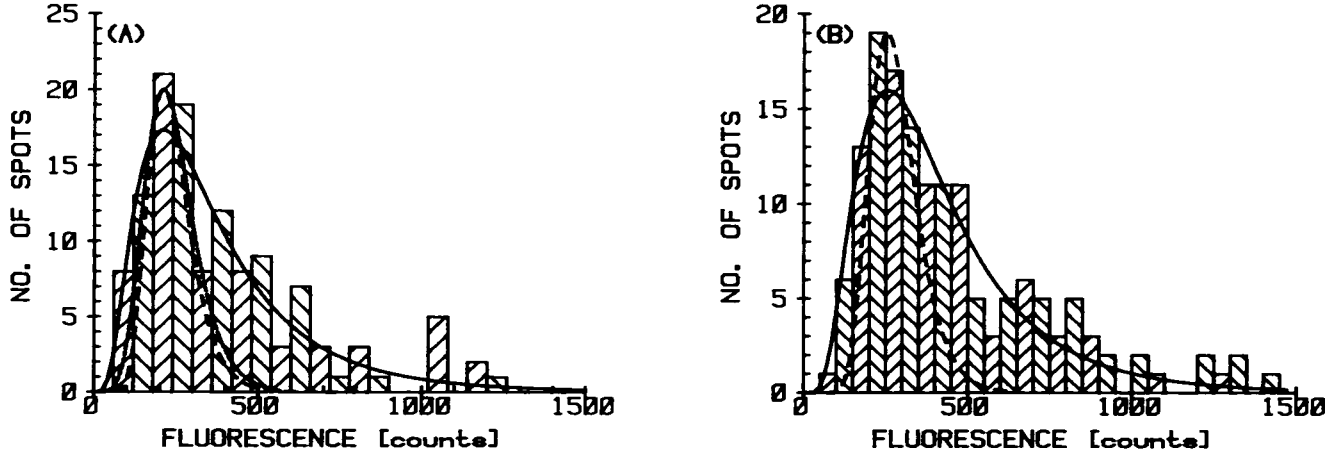

FIGURE 5 Comparison of fluorescence distributions on polylysine-coated slides with surface area distributions for (*A*) dil-LDL and (*B*) R_{18}-virus. The histograms are fluorescence distributions (Fig. 3, *A* and *C*), and the solid lines are best-fit log-normal functions with parameters given in Table 1. The dashed lines are derived from surface area distributions (as shown in Fig. 4) and are best-fit log-normal functions normalized to the same peak positions as the dashed lines. This is convolved with a Poissonian distribution of fluorophore numbers, centered on 40 probes/particle to give the dotted line; in *B*, the convolution with the 200 probes/particle Poissonian is almost coincident with the dashed line.

required to identify and image suitable cells is short compared with preincubation times used for fixed cells by ourselves and others. There were no obvious differences between distributions obtained on fixed cells and on live cells at 4°C.

Visual comparison of the data in Figs. 6 and 3 reveals that the on-cell fluorescence intensity distribution for LDL is significantly broader than the polylysine-coated slide distribution, which is indicative of clustering. The on-cell distribution for influenza virus also appears to be somewhat broadened. Simple log-normal fits to the data gave width parameters that are given in Table 1.

The data were further analyzed by deconvolving the distributions into 1, 2, 3 ... etc. particle components as described under Materials and Methods. The deconvolutions were based on the log-normal fit to the polylysine-coated slide data, which are assumed to correspond to the single particle fluorescence intensity distribution. It was found that the deconvolution yields reasonably accurate values for the numbers of single particles but that large SEs are encountered for the numbers of 2-particle, 3-particle etc. clusters. Accordingly, it is not possible to determine a complete cluster size distribution, although the proportions of single- and clustered particles can be assessed with some confidence. Typical results are given in Table 1.

Time-dependent measurements at 20°C

Changes in the distribution of R_{18}-labeled LDL particles on the surface of D532 and JD cells were followed using the dual temperature control as described in Materials and Methods. The long observation times, up to 40 min, caused some problems as some cells changed shape ("rounded up"), so that the area in sharp focus shrank in size. Thus, the data sets were smaller than ideal; in some cases, only ~150 spots could be used with confidence in the distribution analysis and, thus, the fraction of single-particle spots is subject to large errors.

A typical set of histograms for a D532 cell is shown in Fig. 7, together with the best fits obtained by global analysis, using log-normal distributions with 2- and 3-particle convolutions. The single-particle fraction is plotted in Fig. 8 as a function of time, together with some results for other cells. The zero time point cannot be established with accuracy, because the temperature rise to 20°C takes ~120 s. The best way of evaluating these trends is thus to report the gradient

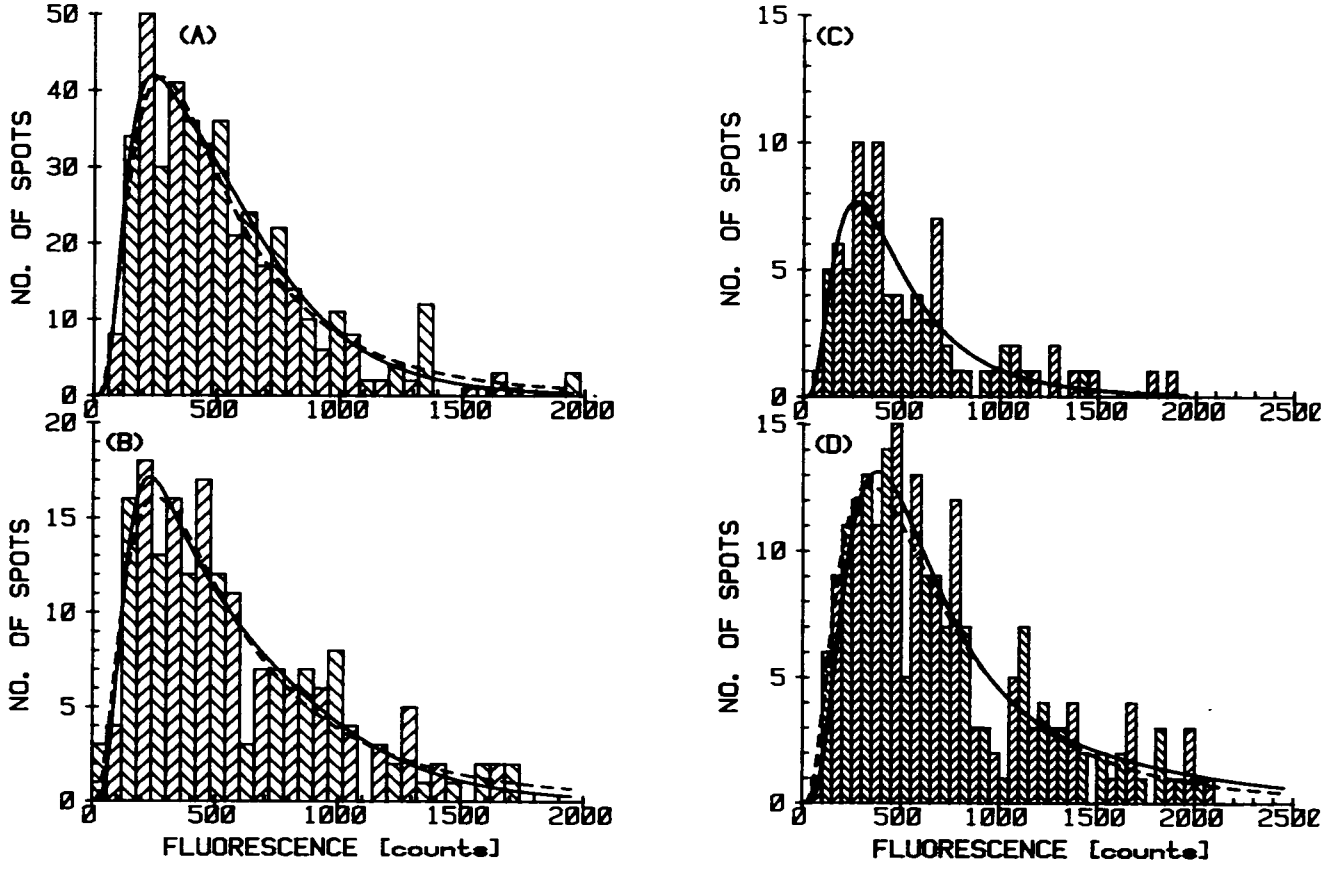

FIGURE 6 Fluorescence intensity distributions for labeled particles on D532 fibroblasts: (*A*) LDL with ~40 dil; (*B*) LDL with ~40 R_{18}; (*C*) virus with ~200 R_{18}/particle; and (*D*) virus with ~1000 R_{18}/particle. The dashed lines are best-fit single log-normal functions, for comparison with Fig. 3 and not intended to represent theoretical distributions; the widths are given in Table 1. The solid lines are 1-particle with 2-particle and 3-particle convolutions, best-fitted using the corresponding polylysine-coated slide distributions as the single particle function; the fit results are shown in Table 1.

TABLE 1 Least-squares parameters for fits to the fluorescence intensity histograms

Section A dil/LDL	Position F_{max}	Width w	No. of spots N_j	No. of spots %	% of particles
On PLCS	209 ± 10 cts	1.89 ± 0.08	122 ± 8		
On cell	270 ± 12 cts	2.05 ± 0.08	443 ± 22		
On cell (convolution)	217 ± 8 cts	1.81 ± 0.06	264 ± 21 174 ± 23 8 ± 28	59 ± 7 39 ± 6 2 ± 7	42 ± 7 55 ± 10 4 ± 8
Section B R_{18}/LDL	**Position F_{max}**	**Width w**	**No. of spots N_j**	**No. of spots %**	**% of particles**
On PLCS	255 ± 9 cts	1.82 ± .05	154 ± 7		
On cell	255 ± 17 cts	2.20 ± .10	191 ± 12		
On cell (convolution)	246 ± 8 cts	1.86 ± .05	132 ± 10 39 ± 14 19 ± 13	69 ± 9 21 ± 8 10 ± 7	49 ± 10 29 ± 9 21 ± 10
Section C R_{18}/virus (200 probes/particle)	**Position F_{max}**	**Width w**	**No. of spots N_j**	**No. of spots %**	**% of particles**
On PLCS	255 ± 8 cts	1.80 ± .05	145 ± 6		
On cell	267 ± 19 cts	1.94 ± .10	86 ± 7		
On cell (convolution)	270 ± 20 cts	1.80 ± .05	78 ± 9 1 ± 12 9 ± 8	89 ± 20 1 ± 12 10 ± 8	73 ± 25 2 ± 16 25 ± 16
Section D R_{18}/virus (1000 probes/particle)	**Position F_{max}**	**Width w**	**No. of spots N_j**	**No. of spots %**	**% of particles**
On PLCS	393 ± 14 cts	1.82 ± .06	371 ± 17		
On cell	339 ± 20 cts	2.1 ± .1	214 ± 12		
On cell (convolution)	378 ± 12 cts	1.89 ± .05	196 ± 15 4 ± 23 19 ± 18	89 ± 15 2 ± 10 9 ± 8	75 ± 21 3 ± 13 22 ± 13

In each section, the first line is the control image of the sample dispersed on a polylysine-coated slide (PLCS), fitted by a single log-normal function (Eq. 3) with width in log(counts) units. The second entry is data for the sample bound to a D532 fibroblast, also fitted by a simple log-normal; the third entry is the same data fitted with a combined 1-, 2-, and 3-particle convolution function (Eq. 6). The widths and positions of the 1-particle function can be seen to correspond closely to those of the control data. The final column gives the relative numbers of LDL or virus particles in the 1-, 2-, and 3-particle clusters.

of the regression line to the data points. These values are given in Table 2.

DISCUSSION

For a population of particles of uniform size, the number of fluorophores per particle and the fluorescence intensity is expected to follow a Poisson distribution. Self-quenching effects might occur, particularly for R_{18} at higher labeling ratios, but these would have the effect of narrowing the fluorescence intensity distribution. In fact, it is clear from Fig.3 that the fluorescence intensity distributions for both LDL and influenza virus are much wider than the Poisson distribution.

To investigate the above discrepancy, we determined LDL and influenza virus particle sizes and calculated their surface area distributions as shown in Fig. 4. Any differences in particle diameter are amplified when the surface areas are calculated. If the surface density of probes is constant, the number of probes per particle might be expected to follow the distribution of surface areas. As shown in Fig. 5, the surface area distributions provide a better account of the fluorescence intensity distributions than does the Poisson distribution, but they are still too narrow. Only a small improvement is obtained by introducing statistical variation in the surface density of probes (Fig. 5 *A*).

It is possible, of course, that the additional broadening of the fluorescence intensity distributions are caused by a degree of microaggregation of the particles. In the case of LDL, however, another explanation can be advanced. Because LDL particles are believed to contain a single copy of apoprotein B-100, it is likely that the fraction of the particle surface occupied by lipid increases with particle size. In this case, larger particles will contain disproportionately more probes. This idea was tested by calculating the expected fluorescence intensity distributions based on the surface area distribution, but assuming that all particles contain only one copy of apoprotein B-100 and, hence, have a constant area

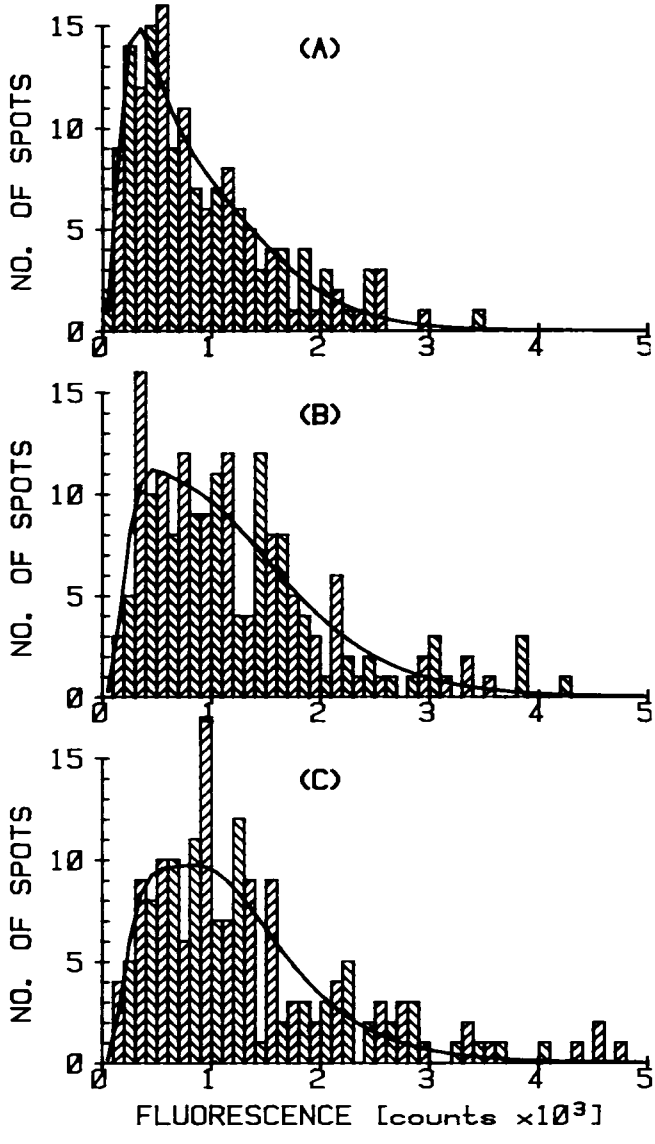

FIGURE 7 Change of fluorescence intensity with time; R_{18}-LDL on D532 fibroblast, measured (*A*) as soon as possible after raising the temperature from 4 to 21°C (*B*) 960 s after *A*, (*C*) 1800 s after *A*. Particles were distinguished from artefacts as described in Materials and Methods; histograms were constructed using the fluorescence signals of spots that passed all three tests. The solid lines are best-fit results of global analysis, using a function of sums of a 1-particle log-normal function with 2- and 3-particle convolutes; fixed photobleaching factors were (*A*) 1.00, (*B*) 1.27, (*C*) 1.37, and the single-particle fractions c_1 were found to be (*A*) 56 ± 10%, (*B*) 44 ± 8%, and (*C*) 43 ± 9%.

unavailable for probe binding. As shown in Fig. 9, a better fit to the experimental distribution is obtained when the surface area occupied by protein is taken to be 600 nm^2 (about 40% of the surface of a 22 nm diameter particle). A calculation using the known proportions of core lipids, phospholipids (assumed to form a monolayer), and protein is in approximate agreement with this value. A similar calculation involving the viral coat proteins would explain the results for influenza virus, but in both cases distortions from probe self-quenching have not been allowed for.

It is worth noting that the comparison between fluorescence intensity distribution and surface area distribution provides reassurance that the imaging system is sufficiently sensitive to detect all particles. If particles of weaker intensity were undetected, the cutoff in the fluorescence intensity distribution would result in a narrower distribution in comparison with the surface area distribution.

The width of the fluorescence intensity distributions for particles bound to polylysine-coated slides has significant consequences for cluster size analyzes. Whatever the precise explanation of the measured distribution, it is reasonable to suppose that this will be the distribution obtained if the particles are bound to single receptors on cell surfaces. We hereafter refer to this distribution as the 1-particle distribution, although recognizing that some contribution from microaggregates is not ruled out. Using a log-normal fit to represent the 1-particle distribution, we calculate the fluorescence intensity distributions for 2-particle, 3-particle, etc. clusters as described in Materials and Methods. In Fig. 10, we show a simulated intensity distribution calculated in this way for a hypothetical distribution of LDL particle clusters. It is evident that the peaks corresponding to the different cluster sizes are very poorly resolved (this is also the case if the 1-particle distribution is based on the surface area distribution of Fig. 3). By comparison, the distribution calculated according to Gross and Webb (1986), who assumed a Poisson distribution for the intensities of individual LDL particles, shows well resolved peaks.

Fig. 6 shows fluorescent intensity distributions of dil- and R_{18}-labeled LDL bound to fibroblasts. The distributions are noticeably broader than for LDL bound to polylysine-coated slides, which is indicative of particle clustering. In agreement with the prediction of Fig. 10, resolved peaks corresponding to individual cluster sizes are not evident.

Our data are at variance with those of Gross and Webb, who did observe multiple peaks in their fluorescence intensity distributions that they interpreted as arising from different sized clusters. We have sometimes observed multiple peaks in data from individual cells, but these are irreproducible and probably caused by statistical fluctuations. As illustrated in Fig. 10, well resolved peaks are only anticipated for particles of uniform size. It is thus difficult to account for the results of Gross and Webb unless their LDL had a much narrower size distribution than is normally encountered.

To quantitate cluster size distributions, we have deconvolved the fluorescent intensity distribution into 1-particle, 2-particle, etc. components as described under Materials and Methods. We find that this analysis gives a good measure of the single particle component but that the statistical uncertainty increases rapidly with cluster size.

The distribution of LDL receptors on the surfaces of fixed cells has previously been studied by electron microscopy using LDL labeled with ferritin (Goldstein, 1979) or colloidal gold (Sanan et al., 1989) or by ^{125}I-LDL autoradiography (Carpentier et al., 1979). After insertion in the plasma membrane, LDL receptors diffuse to coated pits and are endocytosed irrespective of whether LDL is bound (Goldstein,

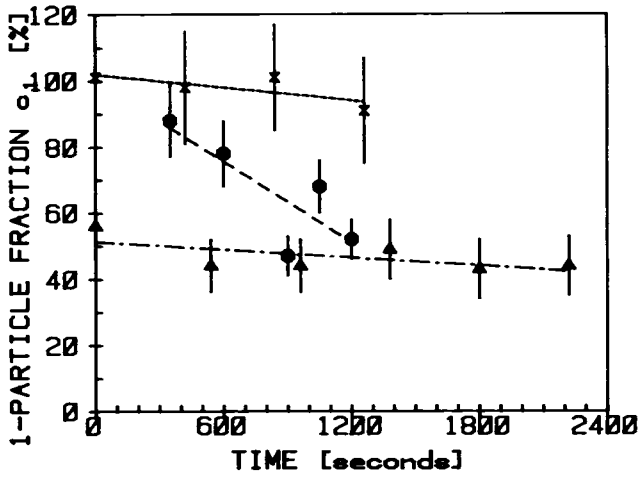

FIGURE 8 Single-particle fractions as a function of time after warming from 4 to 21°C, for populations of R_{18}-LDL on fibroblasts, with best-fit straight lines (parameters given in Table 2). (i) × and short-dashed line: JD cell #5. (ii) ● and dashed line: Detroit 532 cell #2. (iii) ▲ and chained line: Detroit 532 cell #1.

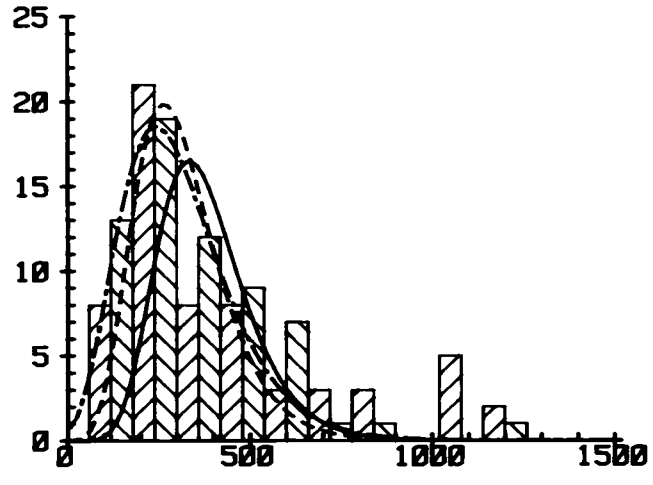

FIGURE 9 Comparison of fluorescence intensity histogram (Fig. 3 *A*) with surface area distribution for LDL with ~40 dil/particle. The solid line is derived from the best-fit of Fig. 4 *A*, convolved with a Poissonian scatter in the number of probes/particle centered on 40 at the median fluorescence value; then normalized in both *x*- and *y*-axes to obtain the minimum residual variance, $RV = 150$. The dashed line is a similar convolution of the surface area best-fit log-normal, but with a constant area of 20% of the median value subtracted to allow for unlabeled (protein) area, and then convolved with the Poissonian; the curve was then renormalized to obtain $RV = 95$. The chained line is as above, but with 40% of the median subtracted as the blocked area, and $RV = 75$. Raising the blocked area fraction to 50% results in the *RV* value increasing again.

1979). At any instant, there is thus a distribution of receptors between coated pits and the rest of the plasma membrane. On normal fibroblasts, the proportion of receptors outside of coated pits varies from 20–50% (Goldstein, 1979). In the fluorescence cluster size analysis, single LDL particles might reasonably be supposed to be principally bound to receptors outside of coated pits. The values in Table 1 are consistent with, although at the upper end of, the electron microscopy data.

Most electron microscopy experiments indicate that recently inserted LDL receptors are randomized in the plasma membrane. Robenek and co-workers have presented conflicting evidence that indicates that LDL receptors are inserted into the plasma membrane as clusters that are not dispersed before their entrapment in coated pits (Robenek et al., 1991; Robenek and Hesz, 1983). Our data, which indicate a high proportion of single LDL particles, support the random distribution model.

It should be recognized that the cluster size distribution of bound LDL particles cannot exactly represent the underlying receptor distribution. To achieve such a correspondence, it would be necessary to saturate the receptors without encountering any nonspecific binding. The average nonspecific binding observed in bulk cell studies with I^{125}-LDL is typically 10–15% of the specific binding at saturation (Goldstein and Brown, 1977). Our observations on single cells also indicate that there is significant nonspecific binding, especially with DiI-labeled LDL, with the added complication that it varies from cell to cell. Any nonspecific binding would probably enhance the proportion of single LDL particles in the cluster size analysis.

Influenza virus binds to sialic acid moieties on the cell surface and, thus, has a wide variety of potential sites of attachment (Marsh, 1984). Its entry into the cell probably occurs as the result of adventitious binding to components that undergo receptor-mediated endocytosis. There is no reason to expect extensive clustering of the viral particles on the cell surface. The cluster size analysis (Table 1) indicates that about 75% of viral particles are present as single particles on the fibroblast surface. Because of the large error, however, the data are also consistent with virtually all of the fluorescent spots corresponding to single particles.

An alternative method, scanning fluorescence correlation spectroscopy (Palmer and Thompson, 1989; St-Pierre and

TABLE 2 Clustering analysis for R_{18}-LDL at 21°C

	D532			JD		
Cell no.	1 (180)	2 (409)	3 (99)	4 (132)	5 (161)	6 (251)
dc_1/dt	−4 ± 3	−41 ± 18	−12 ± 8	10 ± 6	−6 ± 6	−10 ± 5
c_1 (0) %	52 ± 4	101 ± 15	55 ± 9	58 ± 8	102 ± 4	76 ± 7
$\bar{d}_{ss}$ μm	2.3	1.83	2.79	3.48	2.63	3.88

Rate of change of single particle fraction ($10^{-3}s^{-1}$) and value at time zero, with mean nearest neighbour distances $\bar{d}_{ss}$ (microns). In brackets after the cell number is the mean number of spots used per image.

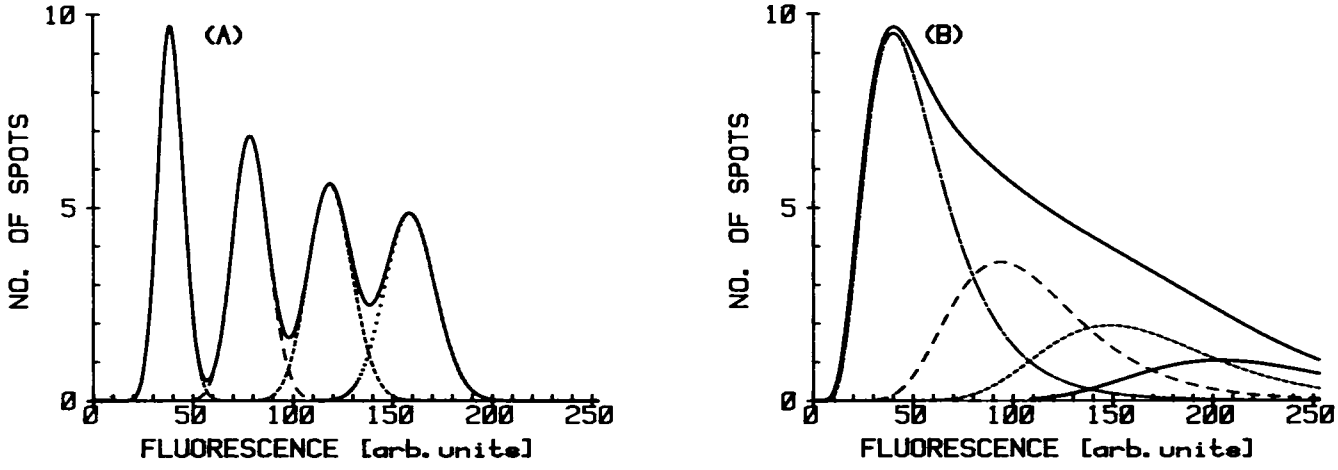

FIGURE 10 Simulated fluorescence intensity distributions. (*A*) Poisson distribution. (*B*) Log-normal distribution with width equal to those found for polylysine-coated slide data for labeled LDL. In each panel, the chained line is the distribution of single particles having a median of 40 probes. The dashed, short dashed, and dotted lines are the 2-, 3-, and 4-particle convolutions, each having the same total intensity as the 1-particle distribution. The solid line is the sum of these individual distributions.

Peterson, 1992; Petersen et al., 1993) can also provide information about the extent of clustering of fluorescently labeled receptors and is less time consuming. However, the low density of the LDL receptor could lead to signal:noise problems if singly labeled antibodies were to be used while the heterogeneously labeled LDL employed in this study would lead to similar difficulty in distinguishing different sized clusters.

Cluster size analyses could conceivably be used to investigate the dynamics of clustering. We have previously reported particle tracking experiments (Anderson et al., 1992) that in principle could give information on the dynamics of receptor clustering through observation of merging of fluorescent particles. However, clustering studies require a high occupancy of receptors to obtain good statistics on the process, but tracking is difficult in such crowded membranes. Thus, we have investigated clustering dynamics by analyzing the shape of the distribution of spot intensities as a function of time, employing global analysis algorithms for fitting the shapes to long tailed theoretical distributions.

To investigate this possibility, we bound R_{18}-LDL to fibroblasts at 4°C and then raised the temperature to 20°C. Images of the same cell were recorded at varying times after raising the temperature and analyzed for cluster size distribution. As a control, we performed identical experiments with JD fibroblasts.

None of the three JD cells examined showed any significant change in the fraction of single particles with time (Table 2). This result is expected because the mutant LDL receptors in these cells do not become entrapped in coated pits (Davis et al., 1986).

Of the three D532 cells examined, two also showed very little change in the fraction of single particles with time. The gradients of the linear regression lines reported in Table 2 were mostly within two SDs of zero, and in these cases the single particle fraction C_1 lies around 50% (Fig. 8). The other normal cell did, however, exhibit a large decrease in C_1 from 90 to 50% in 20 min (Fig. 8). This cell also showed the highest density of LDL-receptors complexes per unit area (Table 2).

It is possible that the observation of time-dependent clustering is sensitive to the density of LDL-receptor complexes. There is evidence (de Brabander et al., 1991; Edidin, 1992; Kusumi et al., 1993) that receptor diffusion can be restricted by domain barriers; our results at 4°C (Anderson et al., 1992) and at 20°C suggest that the dimensions of these domains in D532 cells are of the order of 0.2–1 μm. The rate of clustering would be expected to be greatly reduced for receptors in different domains and, hence, a high concentration of LDL-receptor complexes might be necessary to detect time-dependent changes in cluster size distribution.

Another potentially variable factor is the extent to which the particles were already clustered before measurements were initiated. As pointed out previously, receptors have measurable mobility at 4°C and, thus, LDL-receptor complexes could move sufficiently to precluster in the time interval between binding and the first image acquisition (Anderson et al., 1992). It is possible that cell 2 was particularly favorable for detecting time-dependent clustering because an unusually low proportion of particles appeared to be clustered at the start of the experiment.

Clearly, more experiments are required to establish the conditions under which time-dependent clustering can be measured. The results obtained in this study do, however, suggest that the methodology that we have described may be usefully developed to study the dynamics of receptor clustering on cell surfaces.

We are grateful to the Wellcome Trust and the Science and Engineering Research Council for financial support.

REFERENCES

Anderson, C. M., R. J. Cherry, I. E. G. Morrison, and G. V. W. Stevenson. 1989. Quantification of submicroscopic particles using digital imaging

fluorescence microscopy: application to low density lipoprotein receptors. *Biochem. Soc. Trans.* 17:1100–1101.

Anderson, C. M., G. N. Georgiou, I. E. G. Morrison, G. V. Stevenson, and R. J. Cherry. 1992. Tracking of cell surface receptors by fluorescence digital imaging microscopy using a CCD camera. Low density lipoprotein and influenza virus mobility at 4 C. *J. Cell Sci.* 101:415–425.

Barak, L. S., and W. W. Webb. 1981. Fluorescent low density lipoprotein for observation of dynamics of individual receptor complexes on cultured human fibroblasts. *J. Cell Biol.* 90:595–604.

Bormann, B. J., and D. M. Engelman. 1992. Intramembrane helix-helix association in oligomerization and transmembrane signalling. *Annu. Rev. Biophys. Biomol. Struct.* 21:223–242.

Brown, M. S., S. E. Dana, and J. L. Goldstein. 1974. Regulation of 3-hydroxy-3-methyl-glutaryl coenzyme A reductase activity in cultured human fibroblasts. *J. Biol. Chem.* 249:789–796.

Carpentier, J.-L., P. Gordon, J. L. Goldstein, R. G. W. Anderson, M. S. Brown, and L. Orci. 1979. Binding and internalization of 125 I-LDL in normal and mutant human fibroblasts: a quantitative autoradiographic study. *Exp. Cell Res.* 121:135–142.

Davis, C. G., M. A. Lehrmann, D. W. Russell, R. G. W. Anderson, M. S. Brown, and J. L. Goldstein. 1986. The J. D. mutation in familial hypercholesterolemia: amino acid substitution in cytoplasmic domain impedes internalisation of LDL receptors. *Cell.* 45:15–24.

de Brabander, M., R. Nuydens, A. Ishihara, B. Holifield, K. Jacobson, and H. Geerts. 1991. Lateral diffusion and retrograde movements of individual cell surface components on single motile cells observed with Nanovid microscopy. *J. Cell Biol.* 112:111–124.

Edidin, M. 1992. Patches, posts and fences; proteins and plasma membrane domains. *Trends Cell Biol.* 2:376–380.

Forte, G. M., A. V. Nichols and R. M. Glaeser. 1968. Electron microscopy of human serum lipoproteins using negative staining. *Chem. Phys Lipids.* 2:396–408.

Goldstein, J. L., R. G. W. Anderson, and M. S. Brown. 1979. Coated pits, coated vesicles, and receptor-mediated endocytosis. *Proc. Natl. Acad. Sci. USA.* 279:679–685.

Goldstein, J. L., and M. S. Brown. 1977. The low-density lipoprotein pathway and its relation to atherosclerosis. *Annu. Rev. Biochem.* 46:897–930.

Gross, D. G., and W. W. Webb. 1986. Molecular counting of low-density lipoprotein particles as individuals and small clusters on cell surfaces. *Biophys. J.* 49:901–911.

Hatch, F. T., and R. S. Lees. 1968. Practical methods for plasma lipoprotein analysis. *Adv. Lipid Res.* 6:1–68.

Haugland, R. P. 1989. Molecular Probes Handbook of Fluorescent Probes and Research Chemicals. Molecular Probes Inc., Eugene, OR.

Hillyard, L. A., C. Entmann, H. Feinberg, and I. L. Chaikoff. 1955. Lipid and protein composition of four fractions accounting for total serum lipoproteins. *J. Biol. Chem.* 214:79–90.

Hiraoka, Y., J. W. Sedat, and D. A. Agard. 1987. The use of charge-coupled device for quantitative optical microscopy of biological structures. *Science.* 238:36–41.

Hoekstra, D., T. De Boer, K. Klappe, and J. Wilschut. 1984. Fluorescence method for measuring the kinetics of fusion between biological membranes. *Biochemistry.* 23:5675–5681.

Inoue, S. 1989. Imaging of unresolved objects, superresolution, and precision of distance measurements, with video microscopy. *Methods Cell Biol.* 30:85–112.

Kane, J. P. 1983. Apolipoprotein B: structural and metabolic heterogeneity. *Annu. Rev. Physiol.* 45:637–650.

Knutson, J. R., J. M. Beechem, and L. Brand. 1983. Simultaneous analysis of multiple fluorescence decay curves: a global approach. *Chem. Phys. Lett.* 102:501–507.

Kusumi, A., Y. Sako, and M. Yamamoto. 1993. Confined lateral diffusion of membrane receptors as studied by single particle tracking (Nanovid microscopy). Effects of calcium-induced differentiation in cultured epithelial cells. *Biophys. J.* 65:2021–2040.

Lowry, O. H., N. J. Rosebrough, A. L. Farr, and R. J. Randall. 1951. Protein measurement with the Folin phenol reagent. *J. Biol. Chem.* 193:265–275.

Markwell, M. A. K., S. M. Haas, L. L. Bieber, and N. E. Tolbert. 1978. A modification of the Lowry procedure to simplify protein determination in membrane and lipoprotein samples. *Anal. Biochem.* 87:206–210.

Marsh, M. 1984. The entry of enveloped viruses into cells by endocytosis. *Biochem. J.* 218:1–10.

Metzger, H. 1992. Transmembrane signalling. The joy of aggregation. *J. Immunol.* 149:1477–1487.

Mosteller, M., and J. W. Tukey. 1977. Data Analysis and Regression: A Second Course in Statistics. Addison-Wesley, Reading, MA.

Palmer III, A. G., and A. L. Thompson. 1989. High-order fluorescence fluctuation analysis of model protein clusters. *Proc. Natl. Acad. Sci. USA.* 86:6148–6152.

Petersen, N. O., P. L. Höddelius, P. W. Wiseman, O. Seger, and K.-E. Magnusson. 1993. Quantitation of membrane receptor distributions by image correlation spectroscopy: concept and application. *Biophys. J.* 65: 1135–1146.

Robenek, H., B. Harrach, and N. J. Severs. 1991. Display of low density lipoprotein receptors is clustered, not dispersed, in fibroblast and hepatocyte membranes. *Atherosclerosis and Thrombosis.* 11:261–271.

Robenek, H., and A. Hesz. 1983. Dynamics of low-density lipoprotein receptors in the plasma membrane of cultured human skin fibroblasts as visualized by colloidal gold in conjunction with surface replicas. *Eur. J. Cell Biol.* 31:275–282.

Sanan, D. A., D. R. van der Westhuyzen, W. Gevers, and G. A. Coetzee. 1989. Early appearance of dispersed low density lipoprotein receptors on the fibroblast surface during recycling. *Eur. J. Cell Biol.* 48:327–336.

St-Pierre, P. R., and N. O. Petersen. 1992. Average density and size of microclusters of epidermal growth factor receptors on A431 cells. *Biochemistry.* 31:2459–2463.

Webster, R. G., W. J. Bean, O. T. Gorman, T. M. Chambers, and Y. Kawaoka. 1992. Evolution and ecology of influenza A viruses. *Microbiol. Rev.* 56:152–179.